Two Blocking Sites of Amino-Adamantane Derivatives in Open *N*-Methyl-D-Aspartate Channels

Alexander Sobolevsky and Sergey Koshelev
Institute of General Pathology and Pathophysiology, 125315 Moscow, Russia

ABSTRACT Using whole-cell patch-clamp techniques, we studied the blockade of open *N*-methyl-D-aspartate (NMDA) channels by amino-adamantane derivatives (AADs) in rat hippocampal neurons acutely isolated by the vibrodissociation method. The rapid concentration-jump technique was used to replace superfusion solutions. A kinetic analysis of the interaction of AAD with open NMDA channels revealed fast and slow components of their blockade and recovery. Mathematical modeling showed that these kinetic components are evidence for two distinct blocking sites of AADs in open NMDA channels. A comparative analysis of different simplest models led us to conclude that these AAD blocking sites can be simultaneously occupied by two blocker molecules. The voltage dependence of the AAD block suggested that both sites were located deep in the channel pore.

INTRODUCTION

Earlier it was shown that the interaction of certain compounds with *N*-methyl-D-aspartate (NMDA) channels is complex and cannot be described by a simple one binding site model. The existence of two blocking sites in NMDA channels was established for long-chain adamantane derivatives (Antonov and Johnson, 1996) and *n*-alkyl diamines (Subramaniam et al., 1994). Intracellular and extracellular Mg^{2+} ions blocked the channels interacting with different binding sites (Johnson and Ascher, 1990). Mutagenesis experiments on NMDA receptor subunits showed that Ca^{2+} and Mg^{2+} were likely to bind to multiple sites within the pore that were contributed by both the NMDAR1 and NR2 subunits (MacBain and Mayer, 1994). Spermine and spermidine were suggested to act at distinct sites on NMDA receptors, thereby producing potentiation and block (Rock and MacDonald, 1992; Benveniste and Mayer, 1993; Araneda et al., 1993). The high value of the Hill coefficient ($n_{Hill} > 1$) characterizing the concentration dependence of the block by tetraalkylammonium derivatives (Koshelev and Khodorov, 1992) and bepridil (Sobolevsky et al., 1997) can be considered as evidence in favor of the existence of more than one blocking site for these compounds in NMDA channels. Antonov and Johnson (1996) found that the apparent fractional electrical depth, δ, of the site at which IEM-1754 and IEM-1460 bound to the channel was different for two different ranges of the membrane potential. These different values of δ allowed them to hypothesize the existence of deep and shallow blocking sites for these drugs in NMDA channels. The same assumption could be made for Mg^{2+}, which demonstrated high values of δ: 1.0 (Ascher and Nowak, 1988) and 0.8 (Jahr and Stevens, 1990).

Both parameters, n_{Hill} and δ, proved to have high values for amino-adamantane derivatives (AADs) used in the present study. This fact led us to analyze the AAD-induced kinetics of open channels to verify the hypothesis about the multisite interaction of these compounds with NMDA channels. We actually revealed fast and slow components of channel blockade and recovery, which was in agreement with the two components of recovery from block by memantine and amantadine observed earlier by Johnson et al. (1995). The kinetic analysis described in the present study allowed us to conclude that the AAD-induced block of open NMDA channels was mediated by two distinct blocking sites. These sites are located in the depth of the channel pore and can be simultaneously occupied by two blocking molecules.

MATERIALS AND METHODS

Pyramidal neurons were acutely isolated from the CA-1 region of rat hippocampus by "vibrodissociation techniques" (Vorobjev, 1991). The experiments were begun not earlier than after 3 h of incubation of the hippocampal slices in a solution containing (in mM) 124 NaCl, 3 KCl, 1.4 $CaCl_2$, 2 $MgCl_2$, 10 glucose, 26 $NaHCO_3$. The solution was bubbled with carbogen at 32°C. During the whole period of isolation and current recording, nerve cells were washed with a Mg^{2+}-free solution (in mM): 140 NaCl, 5 KCl, 2 $CaCl_2$, 15 glucose, 10 HEPES (pH 7.3). Fast replacement of superfusion solutions ($\tau < 30$ ms) was achieved using the concentration-jump technique (Benveniste et al., 1990b; Vorobjev, 1991). The currents were recorded at 18°C in the whole-cell configuration, using micropipettes made from Pyrex tubes and filled with an "intracellular" solution (in mM): 140 CsF; 4 NaCl; 10 HEPES (pH 7.2). Electric resistance of filled micropipettes was 3–7 MΩ. Analog current signals were digitized at 1-kHz frequency.

Statistical analysis was performed using the scientific and technical graphics computer program Microcal Origin (version 3.5 for Windows). All of the data presented are mean ± SE; comparisons were made using a paired Student's *t*-test.

Kinetic models used to simulate the AAD action were based on the conventional rate theory and used independent forward and reverse rate constants to simultaneously solve first-order differential equations repre-

Received for publication 10 July 1997 and in final form 20 November 1997.

Address reprint requests to Dr. Sergey Koshelev, Institute of General Pathology and Pathophysiology, Baltiyskaya str. 8, 125315 Moscow, Russia. Tel.: 7-095-155-47-42; Fax: 7-095-151-04-21; E-mail: rans@rans.msk.ru.

0006-3495/98/03/1305/15 $2.00

senting the transitions between all possible states of the channel. The rate constants, k_i ($i = 1, \ldots 4$), were calculated by the method described in Appendix B with the help of Mathcad (version 5.0). Differential equations were solved numerically by using the algorithm analogous to that described previously (Benveniste et al., 1990a).

Amino-adamantane derivatives were synthesized by MERZ (Eckenheimer Landstr. 100–104, 60318 Frankfurt-am-Main, Germany) (see Table 1).

RESULTS

Concentration dependence

Ionic currents through NMDA channels were elicited by fast application of 100 μM aspartate (ASP) in a Mg^{2+}-free, 3 μM glycine-containing solution. At a holding potential of -100 mV, ASP induced an inward current which, after its initial fast rise ($\tau < 30$ ms) up to the value, I_0, indicating the opening of NMDA channels, decreased gradually ($\tau_D = 449 \pm 27$ ms, $n = 21$) down to a certain plateau level, I_S (Fig. 1, *inset*). Such a current decay under continued action of the agonist is a result of desensitization of the receptor-channel complex. The fraction of desensitized channels, $d = 1 - I_S/I_0$, varied between the cells in a wide range of 0.08 to 0.75 and was, on the average, 0.35 ± 0.03 ($n = 23$). AAD inhibited the ASP-induced currents in a concentration-dependent manner. Two-second coapplications of ASP with the blocker were repeated every 3 s up to the point where the plateau current reached its stationary level (I_B). Stationary current responses to MRZ 2/178 at different concentrations are shown in Fig. 1 *A*. The degree of the stationary open-channel block (I_B/I_S) was fitted by the logistic equation (Fig. 1 *B*)

$$\frac{I_B}{I_S} = \frac{A}{1 + ([B]/IC_{50})^{\wedge} n_{Hill}} + \frac{1 - A}{1 + ([B]/IC_{50}^{1})^{\wedge} n_{Hill}^{1}} \quad (1)$$

TABLE 1 Chemical structures of the amino-adamantane derivatives used in the study

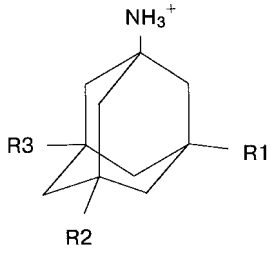

Compound	R1	R2	R3
Memantine	$-CH_3$	$-CH_3$	-H
Amantadine	-H	-H	-H
MRZ 2/150	$-C_2H_5$	$-C_2H_5$	-H
MRZ 2/151	$-C_2H_5$	$-CH_3$	$-CH_3$
MRZ 2/177	$-C_3H_7$ (-isopropyl)	-H	-H
MRZ 2/178	$-C_3H_7$ (-propyl)	-H	-H
MRZ 2/184	$-C_6H_5$	$-C_2H_5$	-H
MRZ 2/239	$-C_3H_7$ (-propyl)	$-C_3H_7$ (-propyl)	-H
MRZ 2/372	$-C_3H_7$ (-isopropyl)	$-C_3H_7$ (-isopropyl)	-H
MRZ 2/457	$-C_2H_5$	$-CH_3$	-H

where $A = 0.79 \pm 0.01$ is the constant, $IC_{50} = 8.7 \pm 0.8$ μM and $IC_{50}^{1} = 0.010 \pm 0.004$ μM are the apparent half-blocking concentrations, $n_{Hill} = 1.26 \pm 0.08$ and $n_{Hill}^{1} = 1.83 \pm 0.99$ are the Hill coefficients, and [B] is the blocker concentration. The concentration dependencies of other AADs were studied at the blocker concentrations in approximately the following range: from 10 times lower to 10 times higher than IC_{50}. The degree of the stationary open-channel block (I_B/I_S) for these blockers was fitted by the following logistic equation:

$$\frac{I_B}{I_S} = \frac{A}{1 + ([B]/IC_{50})^{\wedge} n_{Hill}} \quad (2)$$

The values of the fitting parameters A, IC_{50}, and n_{Hill} are presented in Table 2. It is interesting that the value of A for all AADs proved to be lower than 1. Taking into account the heterogeneity of NMDA channels, this finding can be explained by the existence of another qualitatively different high-affinity binding of AAD to NMDA channels, due to which some of these channels become inactive or blocked.

The kinetics of the open-channel blockade were studied by applying AAD in the continuous presence of ASP (100 μM). Only the cells with parameter d smaller than 0.33 were selected for these experiments. The current traces in response to 5-s applications of MRZ 2/178 at different concentrations are shown in Fig. 2. The blocking as well as the recovery kinetics of current responses were poorly fitted with single exponential functions (Fig. 2 *A*). In contrast, the fittings with double-exponential functions proved to be quite satisfactory (Fig. 2 *B*). The mean values of the amplitude of the fast component, fast and slow time constants, for the blocking (A_{fast}^{on}, τ_{fast}^{on}, and τ_{slow}^{on}, respectively) and recovery kinetics (A_{fast}^{off}, τ_{fast}^{off}, and τ_{slow}^{off}, respectively) of memantine (MEM) and MRZ 2/178 are shown in Fig. 3. Both time constants, τ_{fast}^{on} and τ_{slow}^{on}, decreased with the blocker concentration (Fig. 3, *A* and *C*), whereas τ_{fast}^{off} and τ_{slow}^{off} were practically concentration-independent (Fig. 3, *B* and *D*). The values of the amplitude of the fast component at any two different concentrations were significantly different: A_{fast}^{on} increased ($p < 0.03$) and A_{fast}^{off} decreased with a rise in the blocker concentration ($p < 0.0002$) (Fig. 3, *E* and *F*). For all AADs, in 67% of cells ($n = 69$) A_{fast}^{off} was equal to zero at high blocker concentrations. This fact provides direct evidence that the two components observed in the AAD-induced kinetics cannot be explained by the existence of two different populations of NMDA channels. Otherwise we would observe some fast component, even at infinitely high blocker concentrations. Moreover, two kinetic components were observed in the recovery kinetics of MEM and amantadine in homogeneous NR1a/NR2A and NR1a/NR2B populations of NMDA channels (Blanpied et al., 1997).

According to previous reports (Chen et al., 1992; Parsons et al., 1993, 1995), AADs are uncompetitive NMDA chan-

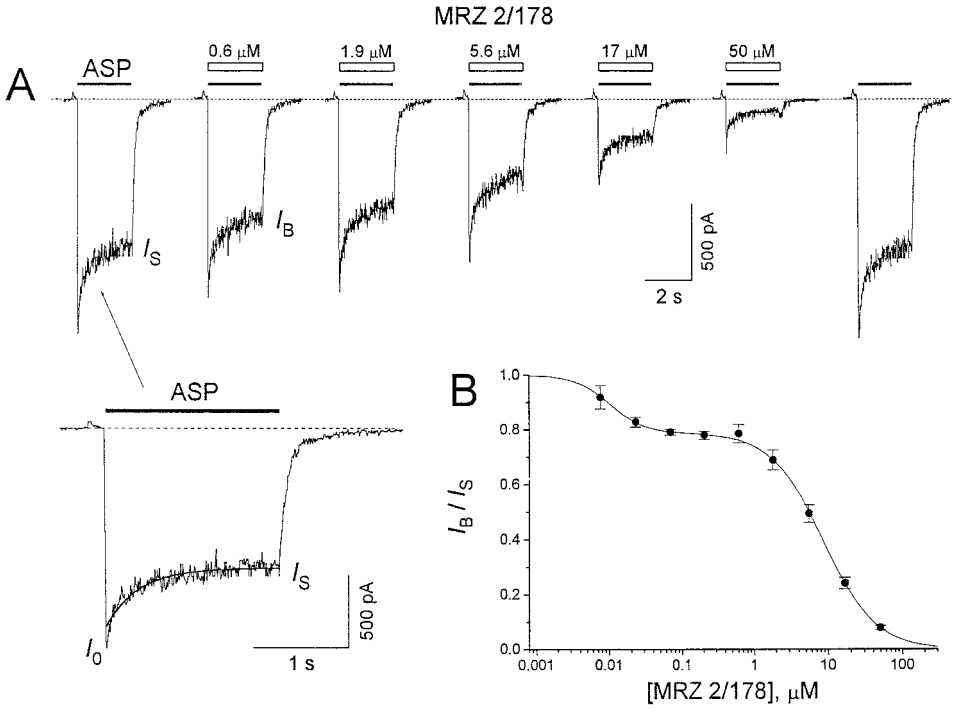

FIGURE 1 Concentration dependence of the stationary NMDA open-channel blockade by MRZ 2/178. MRZ 2/178 at different concentrations was coapplied with ASP (100 μM) for 2 s at −100 mV. (*A*) Stationary NMDA responses in the absence (*first and last traces*) and presence of MRZ 2/178 (0.6, 1.9, 5.6, 16.7, and 50 μM). The inset shows the control response to ASP application on an expanded time scale. The current decrease from I_0 to I_S was fitted with the exponent, τ_D = 320 ms. (*B*) Plateau current responses (I_B) divided by the control plateau value (I_S) were plotted against the MRZ 2/178 concentration. The solid line shows the fitting of the experimental data to Eq. 1. The fitting parameters are A = 0.79 ± 0.01, IC_{50} = 8.7 ± 0.8 μM, n_{Hill} = 1.26 ± 0.08, IC_{50}^1 = 0.010 ± 0.004 μM, and n_{Hill}^1 = 1.83 ± 0.99 (n = 6).

nel antagonists. Their action can be illustrated by a simple one-site model:

$$C \underset{l_2}{\overset{l_1[A]}{\rightleftharpoons}} C_A \underset{\alpha}{\overset{\beta}{\rightleftharpoons}} O_A^* \underset{k_2}{\overset{k_1[B]}{\rightleftharpoons}} O_{AB}$$

Model 1

where C, C_A, O_A, and O_{AB} represent the channel in closed agonist-unbound, closed agonist-bound, open, and open blocked states, respectively. The asterisk indicates the conducting state; l_1, l_2, α, β, k_1 and k_2 are the kinetic constants. [A] is the agonist concentration. Model 1 is a priori unable to explain the existence of two components observed in the open-channel blocking kinetics, because the time constants of the transitions between the C, C_A, and O_A^* states (see Appendix A) are much higher than even fast time constants of the AAD-induced kinetics (Fig. 3, *A–B*).

Is it possible to explain the two components in the open-channel blocking kinetics without the addition to model 1 of another blocked state? Obviously it could be done by taking into account the existence of desensitized states of the channel. For the sake of simplicity, let us consider the model with only one desensitized state (D_A):

$$\begin{array}{ccccc} & & D_A & & \\ & & \gamma \uparrow \downarrow \varepsilon & & \\ C & \underset{l_2}{\overset{l_1[A]}{\rightleftharpoons}} & C_A & \underset{\alpha}{\overset{\beta}{\rightleftharpoons}} & O_A^* \underset{k_2}{\overset{k_1[B]}{\rightleftharpoons}} O_{AB} \end{array}$$

Model 2

The kinetic constants l_1, l_2, α, and β were determined by using the data from literature; and k_1 and k_2 were found

TABLE 2 The concentration and voltage-dependence parameters for AAD

	Concentration dependence			Voltage dependence		
Compound	n_{Hill}	IC_{50} μM	A	δ	$Kd(0)$ μM	A
Memantine	0.92 ± 0.06	0.80 ± 0.21	0.79 ± 0.07	0.73 ± 0.03	18.5 ± 2.7	0.99 ± 0.04
Amantadine	1.02 ± 0.13	14.5 ± 4.4	0.83 ± 0.10	0.92 ± 0.02	737 ± 36	0.99 ± 0.01
MRZ 2/150	1.28 ± 0.13	0.37 ± 0.11	0.79 ± 0.08	0.73 ± 0.07	8.4 ± 2.6	1.04 ± 0.12
MRZ 2/151	1.19 ± 0.15	0.70 ± 0.14	0.75 ± 0.05	1.03 ± 0.12	36.1 ± 14.8	0.83 ± 0.07
MRZ 2/177	1.03 ± 0.07	0.43 ± 0.07	0.85 ± 0.05	0.82 ± 0.03	12.8 ± 1.4	0.95 ± 0.03
MRZ 2/178	1.26 ± 0.08	8.7 ± 0.8	0.79 ± 0.01	0.82 ± 0.08	102 ± 33	0.90 ± 0.09
MRZ 2/184	1.39 ± 0.14	2.49 ± 0.36	0.84 ± 0.04	0.87 ± 0.08	39.3 ± 13.0	1.01 ± 0.10
MRZ 2/239	1.34 ± 0.20	2.78 ± 0.61	0.88 ± 0.04	0.89 ± 0.09	39.2 ± 12.3	0.98 ± 0.08
MRZ 2/372	1.19 ± 0.07	0.72 ± 0.08	0.85 ± 0.02	0.90 ± 0.06	25.6 ± 6.1	0.90 ± 0.05
MRZ 2/457	1.14 ± 0.08	0.39 ± 0.06	0.80 ± 0.03	0.88 ± 0.06	13.4 ± 2.6	0.98 ± 0.05

The values presented are mean ± SE. n = 4–14 cells.

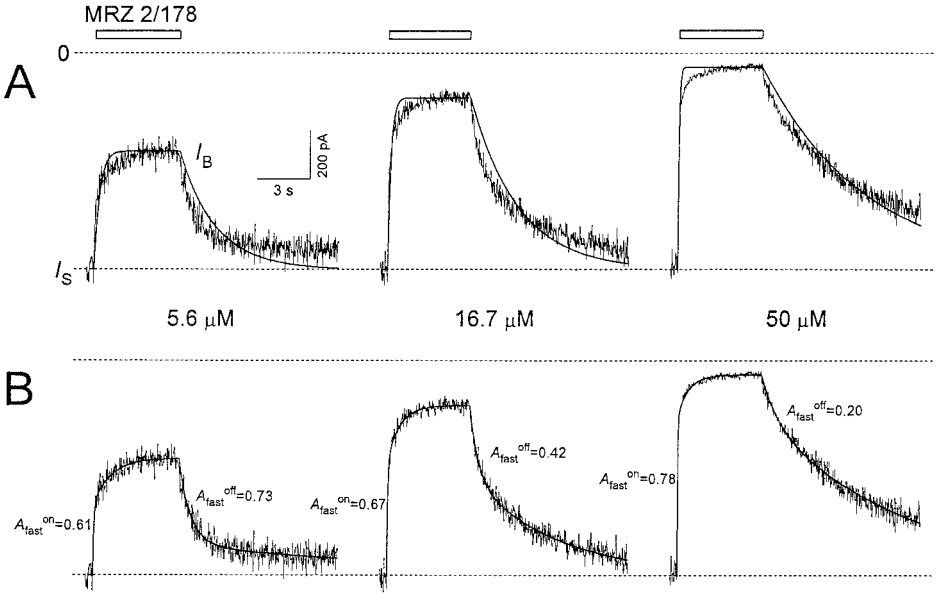

FIGURE 2 The fast and slow components in the kinetics of the NMDA open-channel blockade by MRZ 2/178. ASP (100 μM) was applied continuously. MRZ 2/178 at various concentrations was coadministered for 6 s with ASP. (*A*) Original NMDA responses at the 5.6, 16.7, and 50 μM MRZ 2/178 concentrations were fitted with single exponential functions. (*B*) The same responses were fitted with double exponential functions. The amplitude of the fast component increased with a rise in the blocker concentration for the channels blockade (A_{fast}^{on}) and decreased for their recovery (A_{fast}^{off}).

from the analysis of mean values of τ_{slow}^{on} and τ_{slow}^{off} (Fig. 3, *C* and *D*) for open-channel blockade by MEM and MRZ 2/178 (see Appendix A). The values of γ and ϵ, the rate constants of transitions into and out of D_A, respectively, were defined from the results of studies of control current responses to 2-s ASP application (Fig. 1, *inset*). We found the numerical solutions at different values of *d* (Fig. 4 *A*) and fitted them in the same way as the experimental curves. The modeling values of τ_{fast}^{on}, τ_{fast}^{off}, τ_{slow}^{on}, and τ_{slow}^{off} were of the same range as the experimental ones. A_{fast}^{off}, however, remained constant at different AAD concentrations, irrespective of the *d* value (Fig. 4 *B*). Moreover, at a comparatively low value of *d* (but an extremely high value for kinetic experiments) of 0.32, the fast component of the recovery kinetics was negligible ($A_{fast}^{off} = 0.014$ for MEM and $A_{fast}^{off} = 0.045$ for MRZ 2/178). The Hill coefficient for model 2 is exactly equal to 1 (see Appendix C) and thus cannot explain the experimentally observed values of n_{Hill} exceeding 1.

Thus we failed in our attempt to explain the two components in the open-channel blocking kinetics of AAD by an addition of the desensitized state to one-site model 1. So it is necessary to increase the number of blocked states of the channel. Let us consider the appropriate simplest kinetic models. As the behavior of other parameters predicted by model 2 was qualitatively the same as the experimental one, the main object of our observation will be the behavior of A_{fast}^{off} for the channel recovery from the AAD-induced blockade depending on the blocker concentration. Therefore we have no need to take into account the desensitized states of the channel because, as shown above, the addition of these states to the kinetic model not only leaves A_{fast}^{off} constant at different blocker concentrations but, in our experimental range of *d*, it also allows one to consider it as practically zero. For the sake of simplicity and without any loss for our analysis due to the high value of the opening probability (see Appendix A), the processes of the agonist binding and the subsequent channel opening are represented as a straight transition from the closed state (C) to the open state (O_A).

When only one blocker molecule binds to the channel, there are two simplest possibilities to add one new blocked state to Model 1. The first one can be expressed by a sequential kinetic model:

$$C \underset{l_2}{\overset{l_1[A]}{\rightleftharpoons}} O_A^* \underset{k_2}{\overset{k_1[B]}{\rightleftharpoons}} O_{AB} \underset{k_4}{\overset{k_3}{\rightleftharpoons}} X_B$$

Model 3

X_B can represent the second open (O'_{AB}), desensitized (D_{AB}), or closed (C_B) blocked states of the channel. In the latter case, the blocker can be trapped in the closed channel. The trapping block of NMDA channels by memantine and amantadine was reported earlier (Johnson et al., 1995; Chen and Lipton, 1997). In this case, X_B can be designated as C_B, and the kinetic constant k_4 can be written in more detail as $k_4 = l_1 \cdot [A]$. However, under our conditions of the continuous presence of ASP at a constant concentration (100 μM), this more accurate definition is unimportant. Thus all three possible representations of the sequential model are kinetically equivalent.

Another simplest possibility, adding the second blocking site when only one blocker molecule binds to the channel, can be expressed in the form of a parallel kinetic model:

$$\begin{array}{ccccc} & & O_{AB2} & & \\ & & \Big\uparrow k_3[B] \;\; \Big\downarrow k_4 & & \\ C & \underset{l_2}{\overset{l_1[A]}{\rightleftharpoons}} & O_A^* & \underset{k_2}{\overset{k_1[B]}{\rightleftharpoons}} & O_{AB1} \end{array}$$

Model 4

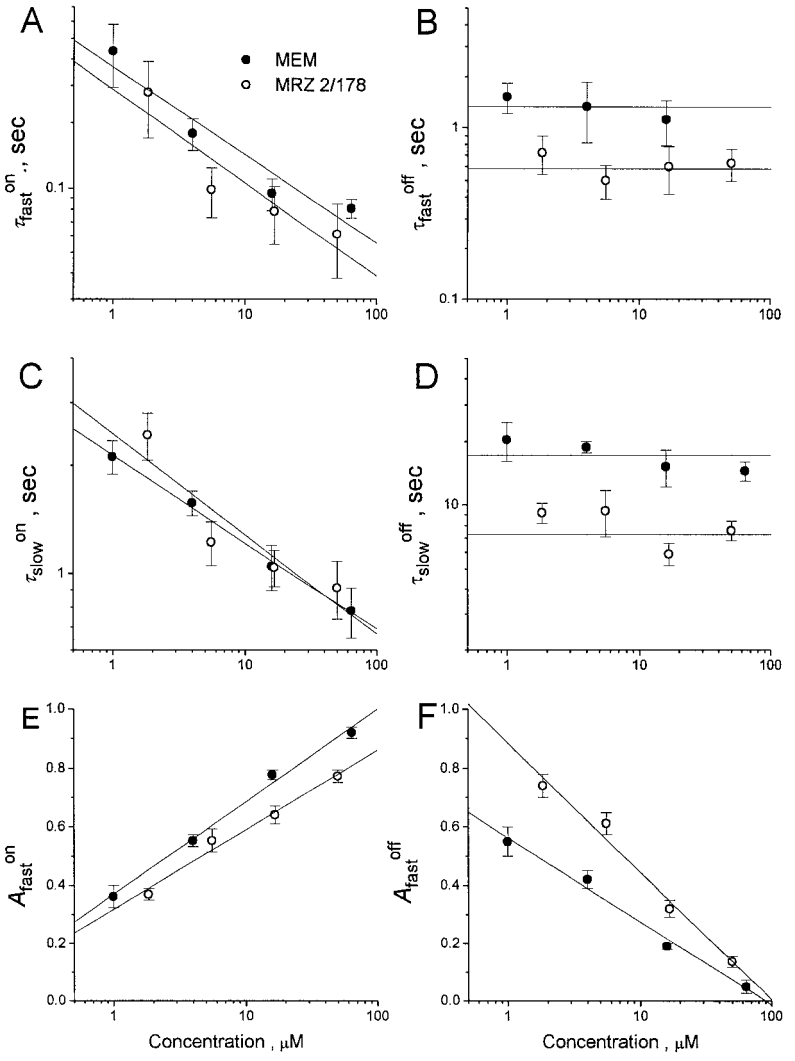

FIGURE 3 The fitting parameters of the kinetics of the NMDA open-channel blockade by MEM and MRZ 2/178 depending on their concentration. The mean fitting parameters for the blocking and recovery phases of the current responses are shown in *A*, *C*, *E* and in *B*, *D*, *F*, respectively. The fast and slow time constants decreased with the blocker concentration for the blockade (*A* and *C*, respectively) and were practically concentration-independent for the recovery (*B* and *D*, respectively). The value of τ_{fast}^{off} for MEM at 64 μM was poorly defined because of the low value of A_{fast}^{off}. The corresponding recovery kinetics were fitted with fixed τ_{fast}^{off} mean for lower MEM concentrations. The amplitude of the fast component increased with the blocker concentration for the channel blockade (*E*) and decreased for their recovery (*F*). The slope of A_{fast}^{off} dependence on the blocker concentration $\Delta A_{fast}^{off}/\Delta[B] = -0.29 \pm 0.02$ ($n = 6$) for MEM, and $\Delta A_{fast}^{off}/\Delta[B] = -0.44 \pm 0.04$ ($n = 5$) for MRZ 2/178.

According to model 4, the blocker binds to one or another blocking site in the channel. The jumps from one blocking site to another are impossible. The kinetic constants for models 3 and 4 (Table 3) were defined unambiguously from the analysis of mean values of τ_{fast}^{on}, τ_{fast}^{off}, τ_{slow}^{on}, and τ_{slow}^{off} (Fig. 3, *A-D*) for the open-channel blockade by MEM and MRZ 2/178 (see Appendix B). Most of the kinetic parameters for both models changed qualitatively in the same way as in the experiment; however, the modeling values of A_{fast}^{off} for the channel recovery from the AAD-induced blockade did not change with the blocker concentration (cf. Figs. 5 and 3 *F*). The inadequacy of these models can also be seen in their inability to explain high experimental values of n_{Hill} (Table 2), because they predict the value of the Hill coefficient as being exactly equal to 1 (see Appendix C).

Model 4 can be complicated by the transition between O_{AB1} and O_{AB2}:

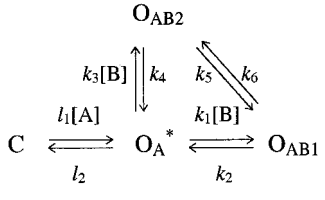

Model 5

TABLE 3 The modeling kinetic constants for MEM and MRZ 2/178

	MEM				MRZ 2/178			
	k_1 $\mu M^{-1}s^{-1}$	k_2 s^{-1}	k_3 $\mu M^{-1}s^{-1}$	k_4 s^{-1}	k_1 $\mu M^{-1}s^{-1}$	k_2 s^{-1}	k_3 $\mu M^{-1}s^{-1}$	k_4 s^{-1}
Model 3	1.92 ± 0.28	0.23 ± 0.02	0.37 ± 0.01	0.158 ± 0.005	0.98 ± 0.42	0.88 ± 0.17	0.73 ± 0.03	0.29 ± 0.06
Model 4	0.24 ± 0.18	0.77 ± 0.07	1.29 ± 0.28	0.056 ± 0.005	0.50 ± 0.27	1.76 ± 0.13	0.48 ± 0.15	0.136 ± 0.019
Model 7	1.15 ± 0.24	0.77 ± 0.07	0.33 ± 0.22	0.056 ± 0.005	0.89 ± 0.37	1.76 ± 0.13	0.080 ± 0.043	0.136 ± 0.019

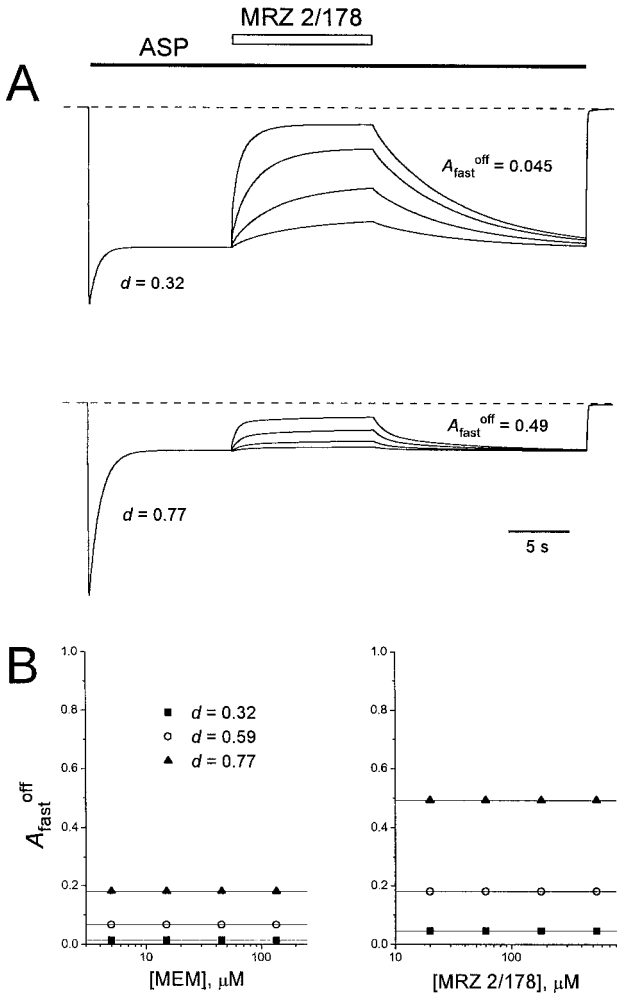

FIGURE 4 The kinetics of responses predicted by model 2. (*A*) MRZ 2/178 at different concentrations (20, 60, 180, and 540 μM) was coapplied with ASP (100 μM) after the agonist-induced current had reached its stationary level. The modeling current traces are presented for two values of the fraction of the desensitized channels, *d*. In both cases the amplitude of the fast component, A_{fast}^{off}, did not depend on the MRZ 2/178 concentration, but increased from 0.045 to 0.49 when *d* rose from 0.32 to 0.77, respectively. (*B*) The values of A_{fast}^{off} for MEM and MRZ 2/178 at different *d* (0.32, 0.59, and 0.77) are plotted against the blocker concentration. Despite the common independence of A_{fast}^{off} on the concentration for MEM and MRZ 2/178, MEM, the blocker slower than MRZ 2/178, demonstrated a lower increase in A_{fast}^{off} with *d*.

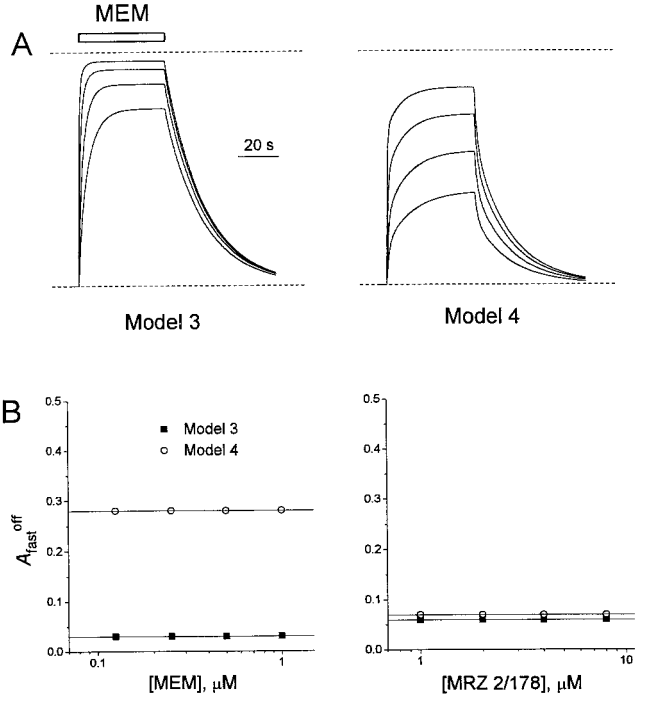

FIGURE 5 The kinetics of responses predicted by models 3 and 4. (*A*) The modeling current traces for models 3 and 4. MEM at different concentrations (0.125, 0.25, 0.5, and 1 μM) was applied in the continuous presence of ASP (100 μM). (*B*) The values of the amplitude of the fast component for the recovery from the block by MEM and MRZ 2/178 for models 3 and 4 were plotted against the blocker concentration. For both models A_{fast}^{off} did not depend on the blocker concentration.

Model 5 describes the situation in which either blocking site can be occupied at first and the blocker can jump from one site to another. As a combination of models 3 and 4, it cannot simulate the experimentally observed kinetics either (Fig. 6). Furthermore, in the framework of the simplest models with two blocked states, the kinetic model can also be complicated by the appearance of two open states of the channel. The existence of two to five conductance levels was shown in experiments with native and recombinant NMDA channels (Gibb and Colquhoun, 1992; Wyllie et al., 1996). This complication of the model can be represented by the following scheme:

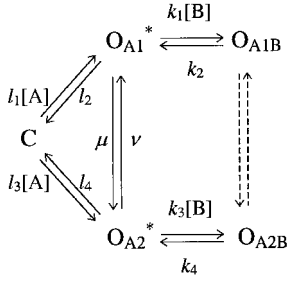

Model 6

where O_{A1} and O_{A2} are the two different open states of the channel and O_{A1B} and O_{A2B} are its blocked states, respectively. Thus the two blocked states in model 6 can correspond to only one binding site of the blocker. The transitions C-O_{A1} and C-O_{A2} are not slower than the transition between C and O_A in model 4 because the mean open time distribution was not shown to contain any components with $\tau > 10$ ms; the transition between O_{A1} and O_{A2} is very fast ($\tau \ll 1$ ms) and, in the majority of NMDA channels, symmetrical (Gibb and Colquhoun, 1992). To our knowledge, the existence of temporal asymmetry was found only for NMDA NR1a/NR2D recombinant channels (Wyllie et al., 1996). Despite the possible asymmetry of the transitions between C, O_{A1}, and O_{A2} with respect to the transitions

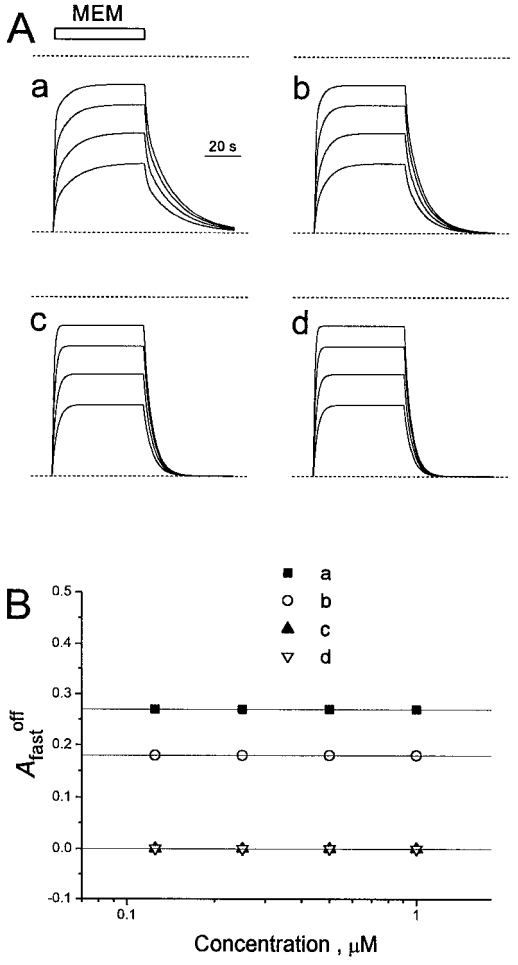

FIGURE 6 The kinetics of responses predicted by model 5. All of the kinetic constants except k_5 and k_6 are the same as for model 4 (see Table 3). The constants k_5 and k_6 are mutually dependent according to the equation $k_1 \cdot k_4 \cdot k_6 = k_2 \cdot k_3 \cdot k_5$. (*A*) The modeling current traces in the cases when the transition between O_{AB1} and O_{AB2} states was (*a*) slower than both O_A-O_{AB1} and O_A-O_{AB2} transitions, $k_5 = 0.006\ s^{-1}$, $k_6 = 0.0153\ s^{-1}$; (*b*) comparable to the slow one, $k_5 = 0.06\ s^{-1}$, $k_6 = 0.153\ s^{-1}$; (*c*) comparable to the fast one, $k_5 = 0.6\ s^{-1}$, $k_6 = 1.53\ s^{-1}$; and (*d*) faster than both of them, $k_5 = 6\ s^{-1}$, $k_6 = 15.3\ s^{-1}$. MEM at different concentrations (0.125, 0.25, 0.5, and 1 μM) was applied in the continuous presence of ASP (100 μM). The recovery kinetics in *a* are practically the same as shown in Fig. 5 for model 4, $\tau_{fast}^{off} = 1.46 \pm 0.01$ s, $\tau_{slow}^{off} = 16.3 \pm 0.1$ s. In *b* the kinetics are faster, $\tau_{fast}^{off} = 1.32 \pm 0.01$ s, $\tau_{slow}^{off} = 9.7 \pm 0.1$ s. In *c* and *d*, the recovery kinetics are single exponential, with the time constants intermediate between the time constants in *a* and *b*. These time constants can be defined as slow; their values were $\tau_{slow}^{off} = 4.69 \pm 0.01$ s and $\tau_{slow}^{off} = 4.09 \pm 0.01$ s for *c* and *d*, respectively. (*B*) The values of the amplitude of the fast component for the recovery from the block by MEM for all four cases described in *A* were plotted against the blocker concentration. In contrast to the experiment, A_{fast}^{off} did not depend on the blocker concentration; it decreased from 0.28 ± 0.01 in *a* to 0.19 ± 0.01 in *b* and became equal to zero in *c* and *d*.

O_{A1}-O_{A1B} and O_{A2}-O_{A2B} due to the different conductance of O_{A1} and O_{A2} states or the temporal asymmetry between them, the rapidity of these transitions provides qualitatively the same kinetics as in the case of models 2–5, i.e., A_{fast}^{off} is concentration-independent (Fig. 7). Model 6 also predicts the value of the Hill coefficient as being exactly equal to 1 (see Appendix C).

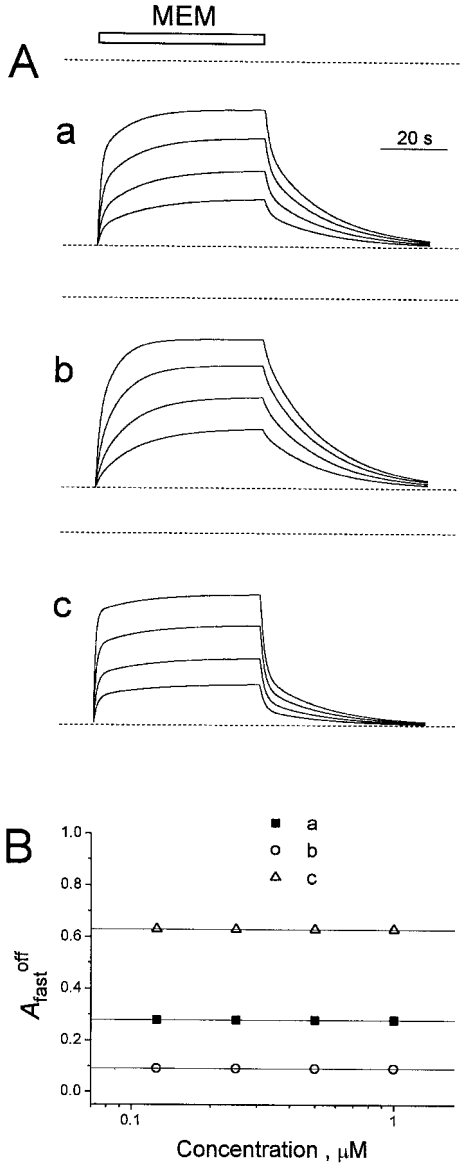

FIGURE 7 The kinetics of responses predicted by model 6. The kinetic constants l_1, l_2, k_1, k_2, k_3, and k_4 are the same as those for model 4 (see Table 3). The constants μ and ν were taken to be high enough to ensure the rapidity of the transition between the O_{A1} and O_{A2} states with respect to the other transitions in model 6 and not too high to simplify the modeling process. The constants l_3 and l_4 were of the same range as l_1 and l_2 and were changed symmetrically with μ and ν to comply with the equation $l_1 \cdot l_4 \cdot \mu = l_2 \cdot l_3 \cdot \nu$. (*A*) The modeling current traces in the cases when the dynamic equilibrium along the transition O_{A1}-O_{A2} was (*a*) symmetrical, $\mu = \nu = 1000\ s^{-1}$, $l_3 = l_1$, $l_4 = l_2$; (*b*) shifted to O_{A1}, $\mu = 4 \cdot \nu = 2000\ s^{-1}$, $l_3 = 2 \cdot l_1$, $l_4 = 0.5 \cdot l_2$; (*c*) shifted to O_{A2}, $\mu = 0.25 \cdot \nu = 500\ s^{-1}$, $l_3 = 0.5 \cdot l_1$, $l_4 = 2 \cdot l_2$. MEM at different concentrations (0.125, 0.25, 0.5, and 1 μM) was applied in the continuous presence of ASP (100 μM). The values of τ_{fast}^{off} and τ_{slow}^{off} were practically the same as for model 4 and did not depend on the blocker concentration. (*B*) The values of the amplitude of the fast component for the recovery from the block by MEM for all three cases described in *A* were plotted against the blocker concentration. A_{fast}^{off} did not depend on the blocker concentration and was the same ($A_{fast}^{off} = 0.28 \pm 0.01$) in *a*, smaller ($A_{fast}^{off} = 0.09 \pm 0.01$) in *b*, and larger ($A_{fast}^{off} = 0.63 \pm 0.01$) in *c* than for model 4 (see Fig. 5 *B*).

Thus no models considered above can qualitatively describe the kinetics of NMDA channel recovery from the AAD blockade. The only way to solve this problem within the framework of simplest models with two blocked states is to suppose that not one, but at least two blocking molecules can simultaneously bind to open NMDA channels. In a kinetic model this fact will be expressed by the appearance of the double-blocked state, O_{AB1B2}. The resulting kinetic model with a double-blocked open-channel state is sequential:

$$C \underset{l_2}{\overset{l_1[A]}{\rightleftharpoons}} O_A^* \underset{k_2}{\overset{k_1[B]}{\rightleftharpoons}} O_{AB2} \underset{k_4}{\overset{k_3[B]}{\rightleftharpoons}} O_{AB1B2}$$

Model 7

Model 7 suggests the strong order for the blocker molecules to occupy their binding sites: site 2 is occupied first, site 1 is occupied thereafter. The constants k_1, k_2, k_3, and k_4 (Table 3) were defined unambiguously according to the experimental kinetics (see Appendix B). Finally, in this case A_{fast}^{off} depends on the blocker concentration qualitatively in the same way as in the experiment: it decreased with concentration for both MEM and MRZ 2/178 (Fig. 8 *A*). It should be noted, however, that the slope of the A_{fast}^{off} dependence on the blocker concentration (Fig. 8 *B*, $\Delta A_{fast}^{off}/\Delta[B] = -0.53 \pm 0.04$ for MEM and $\Delta A_{fast}^{off}/\Delta[B] = -0.61 \pm 0.03$ for MRZ 2/178) was much steeper than that observed in the experiment (Fig. 3 *F*, $\Delta A_{fast}^{off}/\Delta[B] = -0.29 \pm 0.02$ for MEM and $\Delta A_{fast}^{off}/\Delta[B] = -0.44 \pm 0.04$ for MRZ 2/178). It is interesting that taking into account the open probability of less than 1 by involving the closed agonist-bound state of the channel in model 7,

$$C \underset{l_2}{\overset{l_1[A]}{\rightleftharpoons}} C_A \underset{\alpha}{\overset{\beta}{\rightleftharpoons}} O_A^* \underset{k_2}{\overset{k_1[B]}{\rightleftharpoons}} O_{AB2} \underset{k_4}{\overset{k_3[B]}{\rightleftharpoons}} O_{AB1B2}$$

Model 7a

we did not change considerably the recovery kinetics (the values of P_0 were varied by means of variation in β at $\alpha = 200\ s^{-1}$; see Appendix A). Thus the kinetic constants τ_{fast}^{off} and τ_{slow}^{off} remained the same at different P_0. A_{fast}^{off} changed a little with a change in the open probability. The slope of the A_{fast}^{off} dependence on the blocker concentration changed within the error limits (cf. for MEM $\Delta A_{fast}^{off}/\Delta[B] = -0.53 \pm 0.04$ at $P_0 = 1$, model 7, *solid line* in Fig. 8 *B*; and $\Delta A_{fast}^{off}/\Delta[B] = -0.51 \pm 0.03$ at $P_0 = 0.04$, model 7a, *dashed line* in Fig. 8 *B*). Contrary to the kinetics, the concentration dependence of the stationary blockade predicted by model 7a strongly depended on the open probability (Fig. 8 *C*). n_{Hill} increased for MRZ 2/178 from 1.43 ± 0.05 at $P_0 = 1$ (model 7) to 1.81 ± 0.04 at $P_0 = 0.04$ (for MEM $n_{Hill} = 1.60 \pm 0.04$ at $P_0 = 1$ and $n_{Hill} = 1.90 \pm 0.02$ at $P_0 = 0.04$). Thus, in accordance with theoretical predictions (see Appendix C), the modeling kinetics gave n_{Hill} values within the interval from 1 to 2, despite being con-

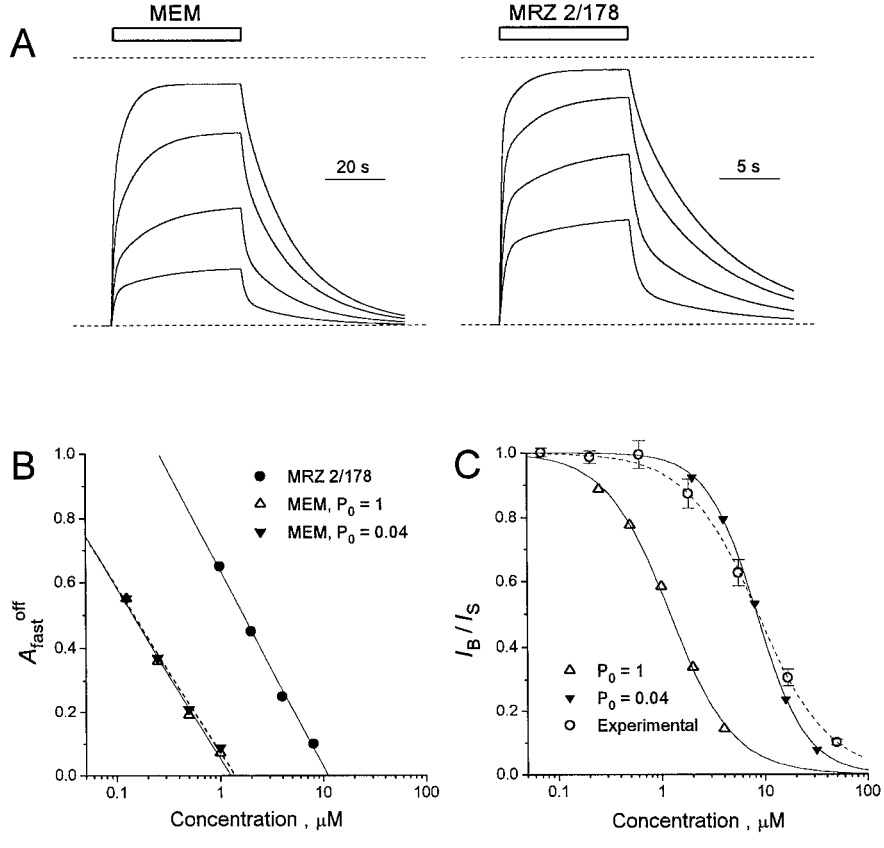

FIGURE 8 The kinetics of responses and the concentration dependence of the stationary blockade predicted by model 7 (7a). (*A*) The modeling current traces predicted by model 7. MEM at concentrations 0.125, 0.25, 0.5, and 1 μM and MRZ 2/178 at concentrations 1, 2, 4, and 8 μM were applied in the continuous presence of ASP (100 μM). (*B*) The amplitude of the fast component predicted by model 7 (7a) at different blocker concentrations. A_{fast}^{off} decreased with the blocker concentration for both MEM and MRZ 2/178. The slope of A_{fast}^{off} dependence on the blocker concentration predicted by model 7 ($P_0 = 1$) was $\Delta A_{fast}^{off}/\Delta[B] = -0.53 \pm 0.04$ for MEM and $\Delta A_{fast}^{off}/\Delta[B] = -0.61 \pm 0.03$ for MRZ 2/178 (shown by *solid lines*). A_{fast}^{off} dependence on the blocker concentration did not practically change when the open probability was decreased according to model 7a (for MEM $\Delta A_{fast}^{off}/\Delta[B] = -0.51 \pm 0.03$ at $P_0 = 0.04$, shown by *dashed line*). (*C*) Concentration dependencies of the stationary blockade by MRZ 2/178 predicted by model 7 ($P_0 = 1$) and model 7a at $P_0 = 0.04$ were superimposed on the normalized concentration dependence observed in the experiment (all of the points except for the two left ones shown in Fig. 1 *B* are represented here). The fittings to Eq. 2 with $A = 1$ of the modeling and experimental data are shown by solid and dashed lines, respectively. The dose-response curve predicted by model 7a was shifted to the right with a decrease in P_0.

siderably larger than those observed in the experiment (Table 2). The value of IC_{50} differed considerably at low and high values of P_0. Thus, for MRZ 2/178, IC_{50} increased from 1.22 ± 0.03 to 8.42 ± 0.10 μM with a decrease in P_0 from 1 to 0.04 (for MEM, $IC_{50} = 0.28 \pm 0.01$ at $P_0 = 1$ and $IC_{50} = 1.63 \pm 0.01$ at $P_0 = 0.04$), and at the low open probability was approximately the same as in the experiment (8.7 ± 0.8 μM).

Potential dependence

The current responses to AAD application in the continuous presence of ASP (100 μM) were different at different membrane potentials (Fig. 9, *inset*). The voltage dependence of the stationary blockade of open NMDA channels by MEM and MRZ 2/178 is shown in Fig. 9. The fitting was done using the equation

$$I_B/I_S = A/(1 + [B]/Kd(0) \times \exp(\delta F E_h/RT)) \quad (3)$$

where A is the constant, E_h is the membrane potential, and $Kd(0)$ is the equilibrium dissociation constant at $E_h = 0$. F, R, and T have their usual meanings. The values of δ, the fraction of the electric field that contributed to the energy of AAD at the blocking sites, proved to be very high (Table 2). The values of A were close to 1.

The double-exponential fit of the 10 μM MEM-induced blocking kinetics (Fig. 10) showed that A^{on}_{fast} decreased at first from 0.79 to 0.54 with an increase in the holding potential from −100 to −40 mV and then was enhanced to 0.65 with a rise in E_h to −20 mV. A^{off}_{fast} for the channel recovery from the MEM blockade increased from 0.27 to 0.79 with an increase in E_h from −100 to −20 mV. The mean values of the amplitude of the fast component, the fast and slow time constants for the blocking, and the recovery kinetics of MEM and MRZ 2/178 depending on E_h are shown in Fig. 11. It should be noted that both time constants, τ^{off}_{fast} and τ^{off}_{slow}, in the kinetics of recovery from MRZ 2/178 decreased with membrane depolarization (Fig. 11, *B* and *D*), whereas in the case of MEM, τ^{off}_{fast} was practically voltage-independent (Fig. 11 *B*). We modeled the kinetics of the AAD interaction with open NMDA channels depending on the membrane potential according to the simplest model 7. As the agonist binding site is considered to be located near the surface of the neuronal membrane, the transition from C to O_A was assumed to be voltage-independent. This assumption can be confirmed by the fact that the whole-cell current-voltage dependence curve in Mg^{2+}-free solutions for NMDA channels is practically linear (Nowak and Wright, 1992; Parsons et al., 1993, 1995) and by the observation that the inhibition of NMDA responses by the competitive antagonists was not voltage-dependent (Benveniste and Mayer, 1991a). The other constants depending on E_h are defined according to the following equations:

$$k_{1(3)} = k^{-100mV}_{1(3)} \exp\left(-\frac{\delta_{1(2)} F \Delta E_h}{2RT}\right) \quad (4)$$

$$k_{2(4)} = k^{-100mV}_{2(4)} \exp\left(\frac{\delta_{1(2)} F \Delta E_h}{2RT}\right) \quad (5)$$

where $k_i^{-100\ mV}$ is the ith kinetic constant at the holding potential of −100 mV, δ_1 and δ_2 are the fractions of the electric field corresponding to the first (from O_A to O_{AB1}) and second (from O_{AB1} to O_{AB1B2}) blocking transitions, and ΔE_h is the difference between E_h and −100 mV. All of the values of the kinetic constants at −100 mV were the same

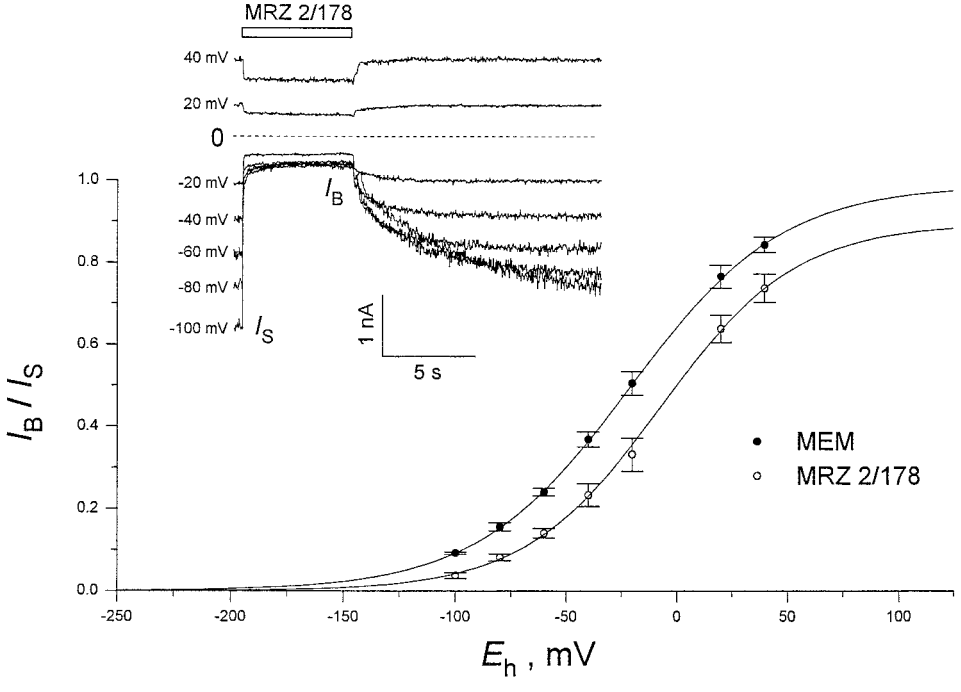

FIGURE 9 The voltage dependence of the stationary NMDA open-channel block by MEM (10 μM) and MRZ 2/178 (80 μM). The stationary current values in the presence of the blocker (I_B) divided by the corresponding control current values (I_S) were plotted against the membrane potential (E_h). The solid lines show the fitting of the experimental data with Eq. 3. The fitting parameters are $A = 0.99 \pm 0.04$, $Kd(0) = 18.5 \pm 2.7$ μM, $\delta = 0.73 \pm 0.03$ ($n = 5$) for MEM, and $A = 0.90 \pm 0.09$, $Kd(0) = 102 \pm 33$ μM, $\delta = 0.82 \pm 0.08$ ($n = 6$) for MRZ 2/178. The inset shows the original current traces at various membrane potentials (from −100 to 40 mV). MRZ 2/178 was applied for 6 s in the continuous presence of ASP (100 μM).

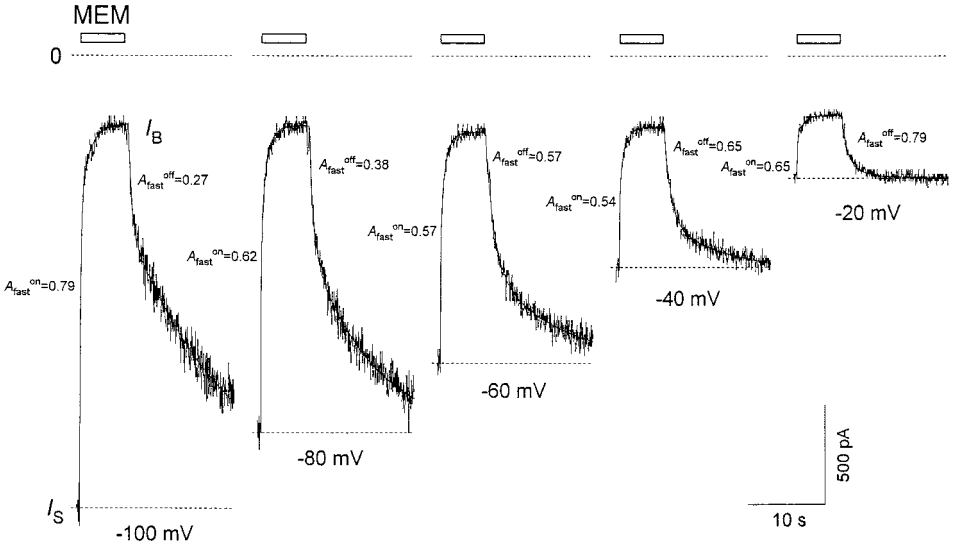

FIGURE 10 The kinetics of the NMDA open-channel block by MEM depending on the membrane potential. ASP (100 μM) was applied continuously. MEM (10 μM) was coadministered for 6 s with ASP at various membrane potentials (from -100 to -20 mV) (E_h). The solid lines show the fitting of the current traces with double exponential functions. The amplitude of the fast component for the channels blockade, A_{fast}^{on}, decreased from 0.79 to 0.54 with an increase in E_h from -100 to -40 mV and then was enhanced to 0.65 with a rise in E_h to -20 mV. A_{fast}^{off} increased from 0.27 to 0.79 with a rise in E_h from -100 to -20 mV.

as in previous experiments with model 7 (Table 3). We considered three different situations for a qualitative kinetic analysis depending on the membrane potential when 1) both the first and second blocking transitions of model 7 ($\delta_1 = 0.45$, $\delta_2 = 0.45$), 2) only the first transition ($\delta_1 = 0.9$, $\delta_2 = 0$), and 3) only the second transition ($\delta_1 = 0$, $\delta_2 = 0.9$) were voltage-dependent. The results of modeling experiments with MRZ 2/178 are shown in Fig. 12 (for MEM the results are qualitatively similar). In the first situation both the fast and slow time constants (τ_{fast}^{off} and τ_{slow}^{off}) for the recovery kinetics decreased with the membrane potential (Fig. 12, *B* and *D*). In the second situation this decrease was observed only for τ_{fast}^{off}, and in the third one, only for τ_{slow}^{off}. A comparison of the τ_{slow}^{off} behavior for the model (Fig. 12 *D*) and the experiment (Fig. 11 *D*) allows one to reject the second situation and to conclude that the second transition in model 7 for both MRZ 2/178 and MEM is potential-dependent. As for the first transition (cf. Fig. 12 and Fig. 11 *B*), the kinetics of MRZ 2/178 indicates that it is strongly voltage-dependent, whereas in the case of MEM the situation remains unclear. A comparison of other kinetic parameters (Fig. 12 and Fig. 11, *A*, *C*, *E*, and *F*) suggests that most probably the first transition for MEM depends on the membrane potential, although to a much smaller degree than for MRZ 2/178.

The voltage dependence of the stationary block by MEM and MRZ 2/178 for model 7 in the three situations mentioned above is shown in Fig. 13. The fit with Eq. 3 gave high values of the integral fraction of the membrane electric field, δ: 0.70 for MEM and 0.66 for MRZ 2/178 in the first situation and 0.90 in the second and third situations for both MEM and MRZ 2/178. Contrary to the first and second cases, in the third case the essential decrease in the limit fraction of unblocked channels at an infinitely high positive potential (parameter *A* in Eq. 3) is observed for both MEM (Fig. 13 *A*, $A = 0.65$) and MRZ 2/178 (Fig. 13 *B*, $A = 0.43$), although in the experiment this value was close to 1 (Table 2). This fact can be considered strong evidence that for all AADs, not only second but also the first transition in model 7 is potential-dependent. Therefore two blocking sites of AADs are located in the depth of the channel pore.

DISCUSSION

In our experiments we studied the concentration- and voltage-dependent blockade of open NMDA channels by AAD. The kinetics of AAD-induced responses in the continuous presence of ASP contained fast and slow components (Fig. 2). This fact is not due to the existence of two different populations of NMDA channels. We made an attempt to explain the appearance of the second kinetic component by the process of desensitization (models 2 and 3), the ability of the channels to close with the blocker inside (model 3), the existence of two different AAD blocking sites on condition that only one blocker molecule can bind to the channel (models 3, 4, and 5), as well as by taking into account multiple open states of the channel (Model 6). However, these attempts failed to model the experimentally observed decrease in A_{fast}^{off} with an increase in the blocker concentration (Fig. 3 *F*). Moreover, the Hill coefficient higher than 1 for practically all AADs (Table 2) cannot be predicted by these models (see Appendix C). The low value of n_{Hill} for MEM can be explained by its ability not only to block NMDA channels but also to potentiate agonist-induced responses (Koshelev et al., 1997). It is clear that any combination of models 2–6 cannot simulate the dependence of A_{fast}^{off} on the blocker concentration or a Hill coefficient higher than 1. Thus the addition of any states to the model will not explain the experimentally observed kinetics on condition that only one blocker molecule can bind to the channel.

The ability of two blocking molecules to bind simultaneously to a NMDA channel and, correspondingly, the appearance in model 7 of the "double-blocked" state allowed us to resolve qualitatively the difficulties mentioned

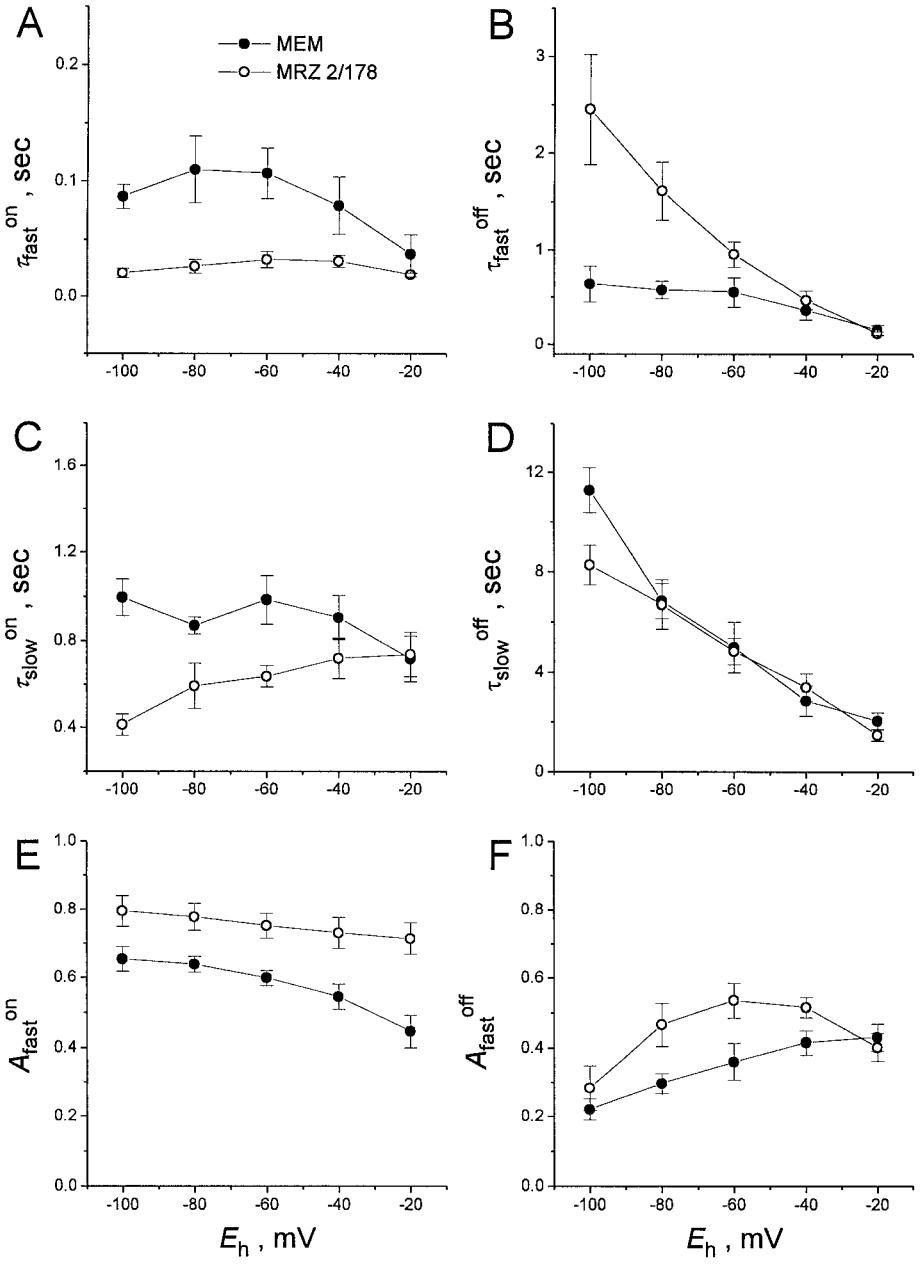

FIGURE 11 The fitting parameters of the kinetics of the NMDA open-channel blockade by MEM and MRZ 2/178 depending on the membrane potential (E_h). The experimental scheme is shown in Fig. 10. The mean fitting parameters for the blocking and recovery phases of the current responses are shown in *A*, *C*, *E* and in *B*, *D*, *F*, respectively. Fast and slow time constants for the recovery from MRZ 2/178 decreased with membrane depolarization (*B*, *D*), whereas in the case of MEM, τ_{fast}^{off} was practically voltage-independent (*B*). The amplitude of the fast component for the recovery from MRZ 2/178 had a nonmonotonous dependence on E_h, whereas A_{fast}^{off} for MEM was enhanced with a rise in E_h (*F*).

above. It is impossible, however, not to notice some quantitative discrepancies: 1) the slope of the A_{fast}^{off} dependence on the blocker concentration (Fig. 8 *B*) is much steeper than that observed in the experiment (Fig. 3 *F*); and 2) the Hill coefficient (Fig. 8 *C*) is much higher than that in the experiment. Furthermore, model 7 is unable to explain the nonmonotonous dependence of A_{fast}^{off} on the membrane potential for the channel recovery from the MRZ 2/178-induced blockade (cf. Figs. 11 *F* and 12 *F*). Evidently, the defects of model 7 are the strict succession, in which two blocking molecules can bind to their sites, and the failure to take into account the trapping block of NMDA channels by AAD. By analogy with Johnson et al. (1995), it is right to suppose that the channel cannot close with the blocker at the shallow site (1), but can do it with the blocker at the deeper site (2). Thus, by adding the new states, O_{AB1} and C_{B2}, to model 7, we obtain the following model:

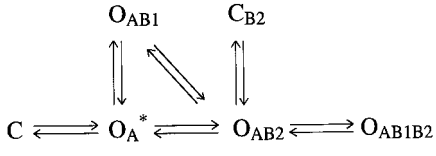

Model 8

which is the combination of models 3, 4, and 7. Unlike model 7, where the first blocking molecule reaches the deep blocking site 2 right from the external solution, model 8 gives this molecule another possibility to gain site 2 by way of sequential "jumps" from the extracellular medium to site 1 and from site 1 to site 2 (Fig. 14). For the sake of

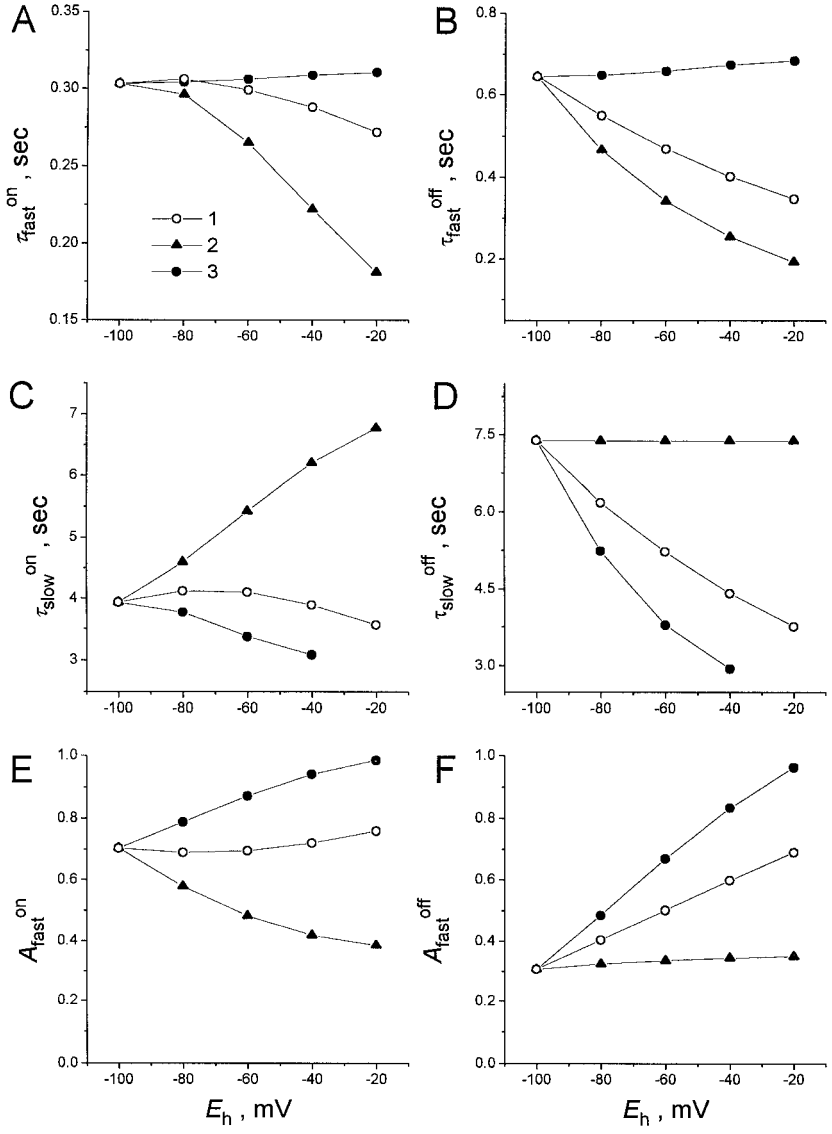

FIGURE 12 The fitting parameters of MRZ 2/178 kinetics depending on the membrane potential (E_h) predicted by model 7. The experimental scheme is the same as that shown in Fig. 5 *A*. The mean fitting parameters for the blocking and recovery phases of modeling responses are shown in *A*, *C*, *E* and in *B*, *D*, *F*, respectively. The fast and slow time constants, and the amplitude of the fast component were plotted against E_h in three following cases when 1) both the first and second blocking transitions of model 7 depended on the membrane potential ($\delta_1 = 0.45$, $\delta_2 = 0.45$); 2) only the first ($\delta_1 = 0.9$, $\delta_2 = 0$) and 3) only the second transition ($\delta_1 = 0$, $\delta_2 = 0.9$) were voltage-dependent. τ_{fast}^{off} for MRZ 2/178 did not decrease with E_h only in situations 3 (*B*), and τ_{slow}^{off} did not decrease with E_h only in situation 2 (*D*). A_{fast}^{off} for MRZ 2/178 did not decrease with E_h in all three situations (*F*). The parameters for the blockade demonstrated qualitatively different voltage dependencies in the three cases considered (*A*, *C*, *E*).

simplicity, this model does not contain all possible desensitized and multiple open states of the channel. Nonetheless, model 8 can predict any slope of A_{fast}^{off} and any value of n_{Hill} intermediate between the values given by models 3, 4, and 7, i.e., it allows one to obtain the correspondence with the experimental values. This model, however, has many more degrees of freedom than the previous ones, and its constants cannot be defined unambiguously from the experimental data.

The potential dependence of the kinetics of AAD-induced responses allows one to understand why such high values of δ were observed for the stationary block of NMDA channels (Table 2). Being some integral fraction of the electric field, δ reflects the penetration of the membrane electric field by two charged blocking molecules up to their binding sites in the pore. Within the framework of model 7, we showed that both blocking sites for MEM and MRZ 2/178 were located in the depth of the membrane electric field. However, site 1 for MEM is located at a point much more shallower than that for MRZ 2/178. Perhaps the long hydrophobic "tail" of MRZ 2/178 promotes the deeper binding of the blocker in the vicinity of site 1 by way of its interaction with the hydrophobic site in the channel pore (Subramaniam et al., 1994).

APPENDIX A

The process of NMDA channel opening consists of two main events: its activation by means of agonists and coagonists binding to their sites and the opening of the gate, which proceeds with the probability P_0. The process of agonist binding was well described by a two-equivalent site model (Benveniste and Mayer, 1991b). Apparent microscopic association and dissociation rate constants for NMDA were determined to be 2.1 s^{-1} μM^{-1} and 24 s^{-1}, respectively. For the single binding site model 1(2), these constants were approximately two times as high. In our modeling experiments the values of dissociation (l_2) and association (l_1) rate constants were taken to be 50 s^{-1} and 4 s^{-1} μM^{-1}, respectively. The choice of the value of α was based on investigations of single NMDA channels (Ascher et al., 1988; Cull-Candy and Usowich, 1989; Jahr and Stevens, 1990). As the mean open time in these works varied from 2.5 to 7 ms, we

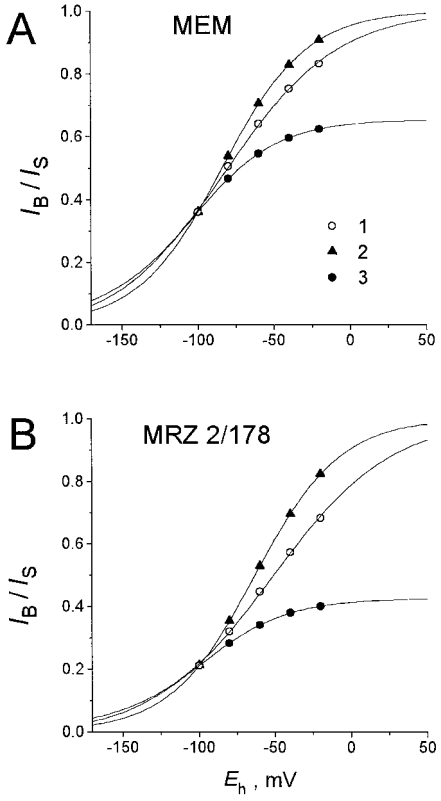

FIGURE 13 The voltage dependence of the stationary block by MEM and MRZ 2/178 predicted by model 7. The experimental scheme is the same as that shown in Fig. 5 *A*. The stationary values of the modeling responses in the presence of MEM and MRZ 2/178 (I_B) divided by the corresponding control values (I_S) were plotted against the membrane potential (E_h) in *A* and *B*, respectively, in three different cases described in Fig. 12. The solid lines show the fitting of the modeling data with Eq. 3. The fitting parameter A is equal to 1 in the first and second situations for both MEM and MRZ 2/178. In the third situation, $A = 0.65$ for MEM and $A = 0.43$ for MRZ 2/178. The parameter δ is equal to 0.70 and 0.66 for MEM and MRZ 2/178, respectively, in the first situation. $A = 0.90$ in the second and third situations for both MEM and MRZ 2/178.

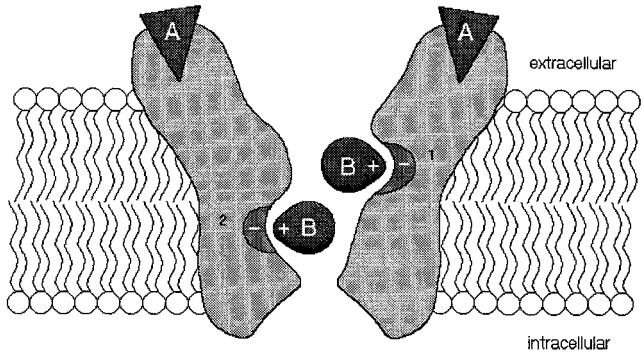

FIGURE 14 The two blocking sites of AADs in the open NMDA channel. The triangles (A) symbolize the molecules of the agonist bound to their sites. The shallow (1) and deep (2) blocking sites of amino-adamantanes are marked by a partial negative electric charge. Both sites are located in the depth of the membrane electric field. According to model 8, the blocker (B) can reach site 2 right from the external solution or by way of sequential "jumps" from the extracellular solution to site 1 and then to site 2. After that, another blocking molecule can occupy site 1. Thus two blocking sites in the open NMDA channel can be occupied simultaneously.

adopted the value of 200 s^{-1} for α. The estimations of the opening probability of the activated channel in the majority of previous studies gave values between 0.2 and 0.5 (Jahr, 1992; Lester et al., 1993; Lin and Stevens, 1994; Benveniste and Mayer, 1995; Colquhoun and Hawkes, 1995), although Rosenmund et al. (1995) showed the low open probability for synaptic NMDA receptor channels. We adopted a value of 0.5. Thus the corresponding value for β proved to be 200 s^{-1}. Taking into account the rapidity of the agonist binding (we used the saturating concentration of ASP, 100 μM) and channel opening, the time constant characterizing the process of desensitization is defined from the equation

$$\tau_D = 1/(\gamma + \epsilon) \tag{A1}$$

where γ and ϵ are the constants for the transition to and from the desensitized state, respectively. The ratio of γ and ϵ can be obtained by using the value $d = I_S/I_0$. At the moment when the control current reaches its maximum value I_0 (see Fig. 1, *inset*), the channels are distributed between states C, C_A, and O_A (model 2) in quasi-equilibrium. Assuming that the sum probability of occupying the states is equal to 1, the probability of occupying the open state will be defined as

$$[O_{A1}] = 1/(l_2\alpha/(l_1[A]\beta) + \alpha/\beta + 1) \tag{A2}$$

At the moment when the control current reaches its stationary value, I_S, we will obtain an equilibrium between states C, C_A, O_A, and D_A. The probability of occupying of the open state will be defined as

$$[O_{A2}] = 1/(l_2\alpha/(l_1[A]\beta) + \alpha/\beta + 1 + \gamma\alpha/\epsilon\beta) \tag{A3}$$

Substituting Eqs. A2 and A3 into the equation

$$I_S/I_0 = 1 - d = [O_{A2}]/[O_{A1}] \tag{4}$$

we obtain the equation for the ratio of γ and ϵ:

$$\gamma/\epsilon = (1/(1 - d))(1 + \beta/\alpha + l_2/(l_1[A])) \tag{A5}$$

Thus, from Eqs. A1 and A5 we define unambiguously the values of γ and ϵ. In accordance with the experiment, the sum of γ and ϵ was taken to be constant (2 s^{-1}), whereas their ratio varied in accordance with different values of d (Eq. A5).

Because of the rapidity ($1/(\gamma + \epsilon) = 0.5$ s) with respect to the slow component of the channel recovery from the AAD blockade ($\tau_{slow}^{off} = 8$ s for MRZ 2/178 and $\tau_{slow}^{off} = 18$ s for MEM), desensitization was proposed to explain the fast component of the AAD-induced kinetics. Then we had to consider the slow component as a result of one-site binding of the blocker to the channel. Thus the association rate constant k_1 was defined from the results of the double-exponential fit (Fig. 3 *C*) by using the equation

$$1/\tau_{slow}^{on} = k_1[B] + k_2 \tag{A6}$$

Mean values of $1/\tau_{slow}^{off}$ for the channel recovery from the AAD-induced blockade (Fig. 3 *D*) gave values of the dissociation rate constant, k_2, according to the equation

$$1/\tau_{slow}^{off} = k_2 \tag{A7}$$

The calculations gave the following values of association and dissociation rate constants: $k_1 = 0.031$ μM^{-1} s^{-1}, $k_2 = 0.056$ s^{-1} for MEM and $k_1 = 0.058$ μM^{-1} s^{-1}, $k_2 = 0.136$ s^{-1} for MRZ 2/178.

APPENDIX B

To solve the linear system of differential equations

$$\frac{dX(t)}{dt} = \mathbf{A}\,X(t) \tag{B1}$$

where $X(t)$ is the vector of variables and **A** is the matrix of constant coefficients, we have to find all of the eigenvalues of **A** by solving the equation

$$|\mathbf{A} - \lambda\mathbf{E}| = 0 \tag{B2}$$

where λ is variable and **E** is the matrix with the diagonal elements equal to 1 and the nondiagonal elements equal to 0. As far as our models are concerned, $X(t)$ represents the vector of probabilities of the channel occupying each of all possible states at time t. **A**, the matrix of transitions between these states, has special properties (Colquhoun and Hawkes, 1977) that allow one to write the solution of Eq. B1 in the following form:

$$X(t) = X(0) \sum_{i=1}^{n} c_i e^{\lambda_i t} \tag{B3}$$

where $X(0)$ is the vector of initial probabilities of the channel state occupancies before the addition or removal of the blocker, λ_i is the ith solution of Eq. B2 or the ith eigenvalue of **A**, and n is the number of states. Each of models 3, 4, and 7 has its own transition matrix with elements representing the sums of the kinetic constants multiplied, where necessary, by the agonist or blocker concentrations. The number of states is equal to 4, and the solution of Eq. B2 gives four values of λ: $\lambda_1 = 0$ and $\lambda_2, \lambda_3, \lambda_4 \neq 0$. Fast channel opening is reflected on one in three nonzero eigenvalues, λ_2, λ_3, and λ_4. Let it be λ_2. Because of its high negative value with respect to the eigenvalues corresponding to the blockade, the second item of the sum in Eq. B3 can be omitted. The values of λ_3 and λ_4 correspond to the fast and slow components of the blocking kinetics at [B] = const. When [B] ≠ 0, we deal with the onset of AAD, and the corresponding eigenvalues, λ_{3ON} and λ_{4ON}, are defined from the blocking kinetics: $\lambda_{3ON} = -1/\tau^{on}_{fast}$ and $\lambda_{4ON} = -1/\tau^{on}_{slow}$. On the contrary, when [B] = 0, we deal with the offset of AAD, and the corresponding eigenvalues, λ_{3OFF} and λ_{4OFF}, are defined from the recovery kinetics: $\lambda_{3OFF} = -1/\tau^{off}_{fast}$ and $\lambda_{4OFF} = -1/\tau^{off}_{slow}$. Thus four equations obtained after substitution of λ_{3ON}, λ_{4ON}, λ_{3OFF}, and λ_{4OFF} into Eq. B2 form a system with four variables: k_1, k_2, k_3, and k_4. The numerical solution of this system of equations gives the values of kinetic constants at every AAD concentration. In the modeling experiments we used the mean values of the constants over the whole range of the blocker concentrations (Table 3).

APPENDIX C

To determine the probability of the channel to be in the open state (O) at equilibrium, the right part of Eq. B1 should be taken as being equal to zero. Thus we obtain the system of n linear equations,

$$\mathbf{A}\,X(t) = 0 \tag{C1}$$

with n variables: $x_1, \ldots, x_n$. However, because of the rank of A equal to $n - 1$, only $n - 1$ equations are independent. Adding the equation for the sum of probabilities of the channel occupying each of all possible states,

$$x_1 + x_2 + \ldots + x_n = 1 \tag{C2}$$

we obtain a system of n equations with n variables. The solutions for our models can be determined analytically. Thus the probabilities of the open state occupancy for models 2, 3, 4, and 7 are

$$[O] = 1/(1 + (\alpha/\beta)(1 + \gamma/\epsilon + l_2/(l_1A)) + (k_1/k_2)[B]) \tag{C3}$$

$$[O] = 1/(1 + l_2/(l_1A) + (k_1/k_2)(1 + k_3/k_4)[B]) \tag{C4}$$

$$[O] = 1/(1 + l_2/(l_1A) + (k_1/k_2 + k_3/k_4)[B]) \tag{C5}$$

$$[O] = 1/(1 + l_2/(l_1A) + (k_1/k_2)[B] + (k_1k_3/k_2k_4)[B]^2) \tag{C6}$$

respectively. The analytically determined values of $[O]_{[B]\neq0}/[O]_{[B]=O}$ at different [B], where $[O]_{[B]\neq0}$ is the probability of the open state occupancy at [B] ≠ 0 and $[O]_{[B]=0}$ is the probability of the open state occupancy at [B] = 0, respectively, give the dependence equivalent to the experimentally obtained concentration dependence of the stationary block (I_B/I_S). The maximum power, to which [B] rises in items of denominators of Eqs. C3–C6, characterizes the Hill coefficient. If this power is equal to 1, the modeling n_{Hill} is equal to 1. Only the denominator of Eq. C6 contains the item with [B] to the second power. The expression for the probability of the open state occupancy for model 6 is too long to be presented here, but the maximum power of [B] is 1. Thus only model 7 can predict a Hill coefficient greater than 1.

The authors thank B. I. Khodorov for critical discussions and helpful comments on the earlier version of the manuscript. We are very grateful to our colleagues at Merz and Co., who kindly supplied us with aminoadamantanes.

This work has been supported by Russian Fund of Fundamental Investigations (no. 96-04-49228).

REFERENCES

Antonov, S. M., and J. W. Johnson. 1996. Voltage-dependent interaction of open channel blocking molecules with gating of NMDA receptors in rat cortical neurons. *J. Physiol. (Lond.).* 493:425–445.

Araneda, R. C., R. S. Zukin, and M. V. L. Bennett. 1993. Effects of polyamines on NMDA-induced currents in rat hippocampal neurons: a whole-cell and single-channel study. *Neurosci. Lett.* 152:107–112.

Ascher, P., P. Bregestovski, and L. Nowak. 1988. *N*-Methyl-D-aspartate-activated channels of mouse central neurones in magnesium-free solutions. *J. Physiol. (Lond.).* 399:207–226.

Ascher, P., and L. Nowak. 1988. The role of divalent cations in the NMDA responses of mouse central neurones in culture. *J. Physiol. (Lond.).* 399:247–266.

Benveniste, M., J. Clements, L. Vyklicky, and M. L. Mayer. 1990a. A kinetic analysis of the modulation of *N*-methyl-D-aspartic acid receptors by glycine in mouse cultured hippocampal neurones. *J. Physiol. (Lond.).* 428:333–357.

Benveniste, M., and M. L. Mayer. 1991a. Structure-activity analysis of binding kinetics for NMDA receptor competitive antagonists: the influence of conformational restriction. *Br. J. Pharmacol.* 40:101–115.

Benveniste, M., and M. L. Mayer. 1991b. Kinetic analysis of antagonist action at *N*-methyl-D-aspartic acid receptors. Two binding sites each for glutamate and glycine. *Biophys. J.* 59:560–573.

Benveniste, M., and M. L. Mayer. 1993. Multiple effects of spermine on *N*-methyl-D-aspartic acid receptor responses of rat cultured hippocampal neurones. *J. Physiol. (Lond.).* 464:131–163.

Benveniste, M., and M. L. Mayer. 1995. Trapping of glutamate and glycine during open channel block of rat hippocampal neuron NMDA receptors by 9-aminoacridine. *J. Physiol. (Lond.).* 483:367–384.

Benveniste, M., J.-M. Mienville, E. Sernagor, and M. L. Mayer. 1990b. Concentration-jump experiments with NMDA antagonists in mouse cultured hippocampal neurons. *J. Neurophysiol.* 63:1373–1384.

Blanpied, T. A., F. Boeckman, E. Aizenman, and J. W. Johnson. 1997. Trapping channel block of NMDA-activated responses by amantadine and memantine. *J. Neurophysiol.* 77:309–323.

Chen, H.-S. V., and S. A. Lipton. 1997. Mechanism of memantine block of NMDA-activated channels in rat retinal ganglion cells: uncompetitive antagonism. *J. Physiol. (Lond.).* 499.1:27–46.

Chen, H.-S. V., J. W. Pellegrini, S. K. Aggarwal, S. Z. Lei, S. Warach, F. E. Jensen, and S. A. Lipton. 1992. Open-channel block of NMDA responses by memantine: therapeutic advantage against NMDA receptor-mediated neurotoxicity. *J. Neurosci.* 12:4427–4436.

Colquhoun, D., and A. G. Hawkes. 1977. Relaxation and fluctuations of membrane currents that flow through drug-operated channels. *Proc. R. Soc. Lond. B.* 199:231–262.

Colquhoun, D., and A. G. Hawkes. 1995. Desensitization of *N*-methyl-D-aspartate receptors: a problem of interpretation. *Proc. Natl. Acad. Sci. USA*. 92:10327–10329.

Cull-Candy, S. G., and M. M. Usowich. 1989. On the multiple-conductance single channels activated by excitatory amino acids in large cerebellar neurones of the rat. *J. Physiol. (Lond.)*. 415:555–582.

Gibb, A. J., and D. Colquhoun. 1992. Activation of *N*-methyl-D-aspartate receptors by L-glutamate in cells dissociated from adult rat hippocampus. *J. Physiol. (Lond.)*. 456:143–179.

Jahr, C. E. 1992. High probability opening of NMDA receptor channels by L-glutamate. *Science*. 255:470–472.

Jahr, C. E., and C. F. Stevens. 1990. A quantitative description of NMDA receptor-channel kinetic behavior. *J. Neurosci.* 10:1830–1837.

Johnson, J. W., S. M. Antonov, T. S. Blanpied, and Y. Li-Smerin. 1995. Channel block of NMDA receptor. *In* Excitatory Amino Acids and Synaptic Transmission. H. V. Wheal, editor. Academic Press, New York. 99–113.

Johnson, J. W., and P. Ascher. 1990. Voltage-dependent block by intracellular Mg^{2+} of *N*-methyl-D-aspartate-activated channels. *Biophys. J.* 57:1085–1090.

Koshelev, S. G., and B. I. Khodorov. 1992. Tetraethylammonium and tetrabutylammonium as tools to study NMDA channels of neuronal membrane. *Membr. Cell Biol.* 9:1365–1369.

Koshelev, S., A. Sobolevsky, and B. Khodorov. 1997. Dual effect of memantine on NMDA channels in acutely isolated rat hippocampal neurones. *J. Physiol. (Lond.)*. 504P:52–53.

Lester, R. A. J., G. Tong, and C. E. Jahr. 1993. Interactions between the glycine and glutamate binding sites of the NMDA receptor. *J. Neurosci.* 13:1088–1096.

Lin, F., and C. F. Stevens. 1994. Both open and closed NMDA receptor channels desensitize. *J. Neurosci.* 14:2153–2160.

MacBain, C. J., and M. L. Mayer. 1994. *N*-Methyl-D-aspartic acid receptor structure and function. *Physiol. Rev.* 74:723–760.

Nowak, L. M., and J. M. Wright. 1992. Slow voltage-dependent changes in channel open-state probability underlie hysteresis of NMDA responses in Mg^{2+}-free solutions. *Neuron.* 8:181–187.

Parsons, C. G., R. Gruner, J. Rozental, J. Millar, and D. Lodge. 1993. Patch clamp studies on the kinetics and selectivity of NMDA receptor antagonism by memantine. *Neuropharmacology.* 32:1337–1350.

Parsons, C. G., G. Quack, I. Bresink, L. Baran, E. Przegalinski, W. Kostowski, P. Krzascik, S. Hartmann, and W. Danysz. 1995. Comparison of the potency, kinetics and voltage-dependency of a series of uncompetitive NMDA receptor antagonists in vitro with anticonvulsive and motor impairment activity in vivo. *Neuropharmacology.* 34: 1239–1258.

Rock, D. M., and R. L. MacDonald. 1992. The polyamine spermine has multiple actions on *N*-methyl-D-aspartate receptor single-channel currents in cultured cortical neurons. *Mol. Pharmacol.* 41:83–88.

Rosenmund, C., A. Feltz, and G. L. Westbrook. 1995. Synaptic NMDA receptor channels have a low open probability. *J. Neurosci.* 15: 2788–2795.

Sobolevsky, A., S. Koshelev, and B. I. Khodorov. 1997. Bepridil-induced blockade of NMDA channels in rat hippocampal neurones. *Neuropharmacology.* 36:319–324.

Subramaniam, S., S. D. Donevan, and M. A. Rogawski. 1994. Hydrophobic interactions of *n*-alkyl diamines with the *N*-methyl-D-aspartate receptor: voltage-dependent and -independent blocking sites. *Mol. Pharmacol.* 45:117–124.

Vorobjev, V. S. 1991. Vibrodissociation of sliced mammalian nervous tissue. *J. Neurosci. Methods.* 38:145–150.

Wyllie, D. J. A., P. Bene, R. S. Nassar, and D. Colquhoun. 1996. Single-channel currents from recombinant NMDA NR1a/NR2D receptors expressed in *Xenopus* oocytes. *Proc. R. Soc. Lond. (Biol.)*. 263: 1079–1086.